Association of *Bacteroides acidifaciens* relative abundance with high-fibre diet-associated radiosensitisation

Chee Kin Then[1]#, Salome Paillas[1]#, Alix Hampson[1], Anne E Kiltie[1]*

[1]CRUK/MRC Oxford Institute for Radiation Oncology, Department of Oncology, University of Oxford

#These authors contributed equally to this work.

*Corresponding author:

Professor Anne E Kiltie

CRUK/MRC Oxford Institute for Radiation Oncology

Department of Oncology, University of Oxford

Old Road Campus Research Building

Off Roosevelt Drive

Oxford OX3 7DQ

anne.kiltie@oncology.ox.ac.uk

+44 1865 617352

Conflict of Interest Statement

The authors have declared that no conflict of interest exists.

Abstract

Patients with pelvic malignancies often receive radiosensitising chemotherapy with radiotherapy to improve survival, at the expense of increased normal tissue toxicity. Other investigators showed slower tumour growth in mice fed high-fibre diets. We hypothesised that mice fed a high-fibre diet would have improved tumour control following ionising radiation (IR) and that this would be mediated through the gut microbiota.

CD1 nude mice were implanted with RT112 human bladder cancer flank xenografts simultaneously with starting a low- or high-fibre (HF; soluble (inulin), insoluble (cellulose) and mixed (50:50)) diet. Significantly higher relative abundance of *Bacteroides acidifaciens* was seen in the gut (faecal) microbiome of the soluble HF group after 2 weeks of diet, by 16S rRNA sequencing ($p<0.01$). Soluble HF resulted in delayed time to treble tumour volume after IR compared to the other groups (8 mice per group, $p=0.005$). Within the soluble HF group, responders to IR (n=4) had significantly higher abundance of *B. acidifaciens* than non-responders (n=4) ($p<0.05$). When all mice fed with different diets (n=32) were pooled, an association was found between the survival time of mice and relative abundance of *B. acidifaciens* ($R^2=0.5278$, $P<0.001$). Our findings might be exploitable for improving radiotherapy response in human patients.

Introduction

Patients with pelvic tumours, including bladder, cervix and rectal cancers, who are receiving radiotherapy are often given additional radiosensitising chemotherapy to improve cure rates, at the expense of increased toxicity in local organs and tissues (1,2). With an ageing population, new approaches to radiosensitisation are urgently required. One such approach might be to modify the intake of dietary fibre by supplements before and during radiotherapy or current standard chemoradiation schedules, which would be a very cost-effective strategy, not expected to add to normal tissue toxicity (3,4).

Wei *et al* showed slower growth rates of subcutaneous lymphoma xenografts in mice fed a high fibre diet (8%) compared to mice on a low-fibre diet, with similar findings in both immune-deficient and immune-competent models (5). This was associated with increased plasma and tumour butyrate levels, but the authors did not investigate the effects of the diet on the gut microbiome.

Dietary fibre manipulation can very rapidly alter the human gut microbiome, with changes in faecal short chain fatty acid (SCFA) levels seen only one day after the diet reaches the distal gut (6). Dietary fibre can also mediate systemic immune effects (7), as can the microbiota-derived SCFAs (8,9). Furthermore, dietary fibre structures align with phenotypes of specific microbes that differ in their metabolic pathways (10). SCFAs are known to confer anti-cancer effects (5,8,9). Other metabolites, including small intermediate and end by-products of endogenous metabolic pathways, products of microbe-host co-metabolism and exogenous signals arising from diet, drugs and other environmental stimuli might also be important (11).

We hypothesised that systemic effects of altered metabolites secreted by gut bacteria on tumours, due to dietary fibre modification, could be exploited in conjunction with ionising radiation (IR) to achieve radiosensitisation.

The aims of this study were to examine the impact of the diet on the microbiome before and after irradiation, and to correlate diet-induced microbiome changes with tumour growth and response to radiation treatment.

Results

The environmental microbiome had minimal impact on gut microbiome analysis

Female CD1 nude mice were injected subcutaneously with RT112 bladder carcinoma cells, and, at the same time, they commenced a modified diet, namely, one of the following: low dietary fibre (0.2% cellulose), low fibre with butyrate in drinking water, high soluble fibre (10% inulin), high insoluble fibre (10% cellulose) and high mixed fibre (5% cellulose, 5% inulin) (Figure 1A and Table S1). We quantified bacterial loads using PCR and gel electrophoresis, compared to known numbers of *E. coli* colony forming units (CFU). Our mouse samples contained more than 10^4 bacterial CFUs which appeared to override contaminating species in the sample microbial communities (Figure 1B). The PBS negative control was processed from the start of the DNA extraction identically to the luminal contents and tissue samples. The amount of nucleic acid detected in the PBS negative controls was extremely low, compared to that in the gut microbiota (Figure 1C). Furthermore, the community microbiome in this negative control differed markedly from the gut microbiome of the mice (Figure 1D). Therefore, the environmental microbiome had minimal impact on the analysis of the gut microbiomes of interest in this study.

The landscape, diversity and enrichment of bacterial taxa in the gut microbiome samples collected when the tumours reached 50 mm^3

In samples collected when the tumours reached 50 mm^3 and 350 mm^3, the faecal (hereinafter referred to as “gut microbiome”) and caecal microbiome were found to have similar bacterial components (Figure S1). In mice culled when their tumours reached 50 mm^3, butyrate levels in the faeces, measured by high-performance liquid chromatography (HPLC), were found to be in the mM range, and were generally higher in the low fibre with

butyrate and high soluble fibre groups (p=NS; Figure S2A). The mean time for tumours to reach 50 mm^3 was 12.8 $\pm$ 1.4 days (Figure S2B).

In faeces collected from culled mice when the tumours reached 50 mm^3, abundance analysis revealed the five bacterial taxa with the highest abundance were *Bacteroides acidifaciens*, *Parabacteroides*, *Akkermansia muciniphila*, *Lachnospiraceae* and *S24-7* (Figure 2A). In terms of alpha diversity, the soluble high fibre group had a lower Shannon's index ($p<0.001$) (Figure 2B). This could be due to the higher abundance of *B. acidifaciens,* which lowered the diversity within groups. In terms of beta diversity, principal coordinate analysis showed a notable cluster effect among different groups, which indicates that samples within groups were more similar to each other than to those from the other groups (Figure 2C). This suggested that the gut microbiome was indeed modified in this study, which might be a diet-effect or a cage-effect (see later). Regarding the abundance of specific taxa in different diet groups (Figure 2D), the high soluble fibre diet significantly increased *B. acidifaciens* abundance ($p<0.001$); the low fibre diet increased *Parabacteroides* abundance ($p<0.001$), the low fibre diet with added butyrate increased *Akkermansia muciniphila* abundance ($p<0.001$), and the high mixed fibre diet increased *Lachnospiraceae* abundance ($p=0.005$).

The landscape, diversity and enrichment of bacterial taxa in the gut microbiome samples collected when the tumours reached 350 mm^3

When the tumours reached 350 mm^3, abundance analysis of the gut microbiome of both IR and non-IR cohorts revealed that the top 6 bacterial taxa with the highest abundance were *S24-7, Akkermansia muciniphila, Bacteroides*, *Lachnospiraceae, Clostridiales* and *B.*

acidifaciens (Figure 3A). In terms of alpha diversity, the soluble HF group had a significantly lower Shannon's index ($p<0.001$ for Kruskal-Wallis test) (Figure 3B). In terms of beta diversity, principal coordinate analysis using Bray-Curtis dissimilarity showed a notable clustering effect among different groups, which indicates that samples within groups were more similar to each other than to those from the other groups (Figure 3C). The composition of the gut microbiome continued to evolve on the diets to the time the tumours reached 350 mm^3, regardless of whether the mice were irradiated or not. The taxonomic cladogram of LEfSe (Linear discriminant analysis Effect size) of the gut microbiome showed that the high soluble fibre diet increased relative abundance of *S24-7* (Figure S3). *B. acidifaciens*, an acetate-producing bacteria (12,13), was found to be of highest abundance in all but the LF diet group at 50 mm^3, but by 350 mm^3 was evenly distributed across the different diet groups, except the soluble HF group treated with radiation ($p=0.200$ for Kruskal-Wallis test) (Figure 3D).

Bacteroidales S24-7 was the highest abundance bacterial taxa in the second cohort. Its relative abundance was significantly higher in the mixed HF and soluble HF groups compared to the LF and insoluble HF group ($p=0.001$ for Kruskal-Wallis test) (Figure 3E).

Soluble high fibre causes increased growth delay in irradiated bladder cancer cell xenografts and responses are influenced by gut microbiota composition

To investigate the effect of different diets on the tumour response in mice irradiated when the tumour had grown to 50 mm^3, tumour growth was monitored to 350 mm^3. Slopes of the tumour growth curves were obtained using linear regression to indicate the tumour progression rates (Figure 4A). The high soluble fibre diet group had the slowest tumour

growth rate. The slopes were 4.4 ± 1.3 for LF, 16.1 ± 1.7 for mixed HF, 28.7 ± 1.3 for insoluble HF and 0.4 ± 1.5 for soluble HF (Figure 4A and Figure S4 for individual irradiated mouse tumour growth curves). Kaplan Meier survival curves for time to treble tumour volume showed that the soluble HF group had the longest median survival time (7.5 days for LF, 7 days for mixed HF, 10 days for insoluble HF, 11.5 days for soluble HF; p=0.005, log-rank test) (Figure 4B).

Among the eight mice fed the soluble high fibre diet, four mice were classified as responders as, using linear regression, they had shallower slopes to the tumour growth curves, namely, 7.3 ± 1.2, -0.9 ± 0.6, -4.8 ± 0.5, -5.2 ± 0.9. The other four mice were classified as non-responders with steeper slopes to the tumour growth curves, namely 34.6 ± 3.0, 31.1 ± 2.6, 23.3 ± 1.0, 33.8 ± 2.9 (Figure 4C). In terms of alpha diversity, there was no significant difference in Shannon's index between responders and non-responders (Figure 4D). In terms of beta diversity, principal coordinate analysis of Bray-Curtis dissimilarity showed the gut microbiome of responders and non-responders were more similar within groups than between groups (Figure 4E).

Differences in composition of the gut microbiome between responders and non-responders

Linear discriminant analysis showed that mice responding to the soluble high fibre diet with a slower tumour growth rate were enriched with *Bacteroidaceae (f), Flavobacterium (g), Flavobacteriales (o), Lactococcus (g), Streptococcus (g), Streptococcaceae (f), Allobaculum (g), Erysipelotrichales (o).* The non-responding tumour-bearing mice were enriched with *Bifidobacterium (g), Bidifobacteriaceae (f), Bifidobacteriales (o), Parabacteroides (g),*

Porphyromonadaceae (f), Lactobacillus (g), Lactobacillaceae (f), and *Lactobacillales* (Figure 5A). In terms of effect size, *B. acidifaciens (sp)* and *Bacteroidaceae (f),* had the largest enrichment in responders, and *Parabacteroides (g),* and *Porphyromonadaceae (f),* had the largest enrichment in non-responders (Figure 5B). To further explore these findings, the discrete false-discovery rates within all taxonomic levels were calculated (Figure 5C). In responders, *B. acidifaciens* species and the *Allobaculum* genus and in non-responders *Lactobacillus* and *Parabacteroides* genera had p-values <0.05 The *B.acidifaciens* abundance was significantly higher in responders than that in non-responders (p=0.029 (Figure 5D), while the *Bacteroidales S24-7* abundance was similar between responders and non-responders in the soluble HF group (p=0.200) (Figure 5E).

Correlation between the abundance of *B. acidifaciens* or *Parabacteroides* genus and mouse survival time in IR and non-IR cohorts

As *B. acidifaciens* was the 'top hit' for responders and the *Parabacteroides* genus was one of the top two 'hits' for non-responders in the soluble HF group, we explored how specific bacterial taxa affected mouse survival time. The correlation between *B. acidifaciens* abundance and time to culling was investigated across the diet groups. Some mice in the non-IR cohort lived as long as those in the IR cohort, ie. >40 days, which may be a reflection of 6 Gy being a relatively low dose of radiation. In the IR cohort, the time of culling positively correlated with *B. acidifaciens* abundance (R^2=0.528, p<0.001). However, a similar correlation was not seen in the non-IR cohort (R^2=0.085, p=0.357) (Figure S5A). Using the time for tumours to treble in volume as the outcome measure, mice with high *B. acidifaciens* abundance had a significantly prolonged median survival time (Log-rank test: p<0.001) (Figure 6A). A similar finding was seen in the IR cohort (p=0.003), but not in the

non-IR cohort (p=0.236). In the IR cohort, the time to culling negatively correlated with the abundance of *Parabacteroides* genus (Figure S5B; R^2=0.164, p=0.022). However, a similar correlation was not seen in the non-IR cohort (R^2=0.084, p=0.360). Mice in the low *Parabacteroides* genus abundance group had no significant difference in median time to treble in volume compared to the high abundance group (Log-rank test: p=0.374) (Figure 6B). *B. acidifaciens* (p=0.200 for Kruskal-Wallis test) and *Parabacteroides* genus (p=0.005 for Kruskal-Wallis test) abundance was evenly distributed among all cages, which suggested that the existence of these taxa in the gut microbiome was not a cage-specific effect (Figure S6 and Table S2).

Metagenomics functional prediction of the gut microbiome by response in the soluble HF group

Functional prediction at KEGG (Kyoto Encyclopedia of Genes and Genomes) pathway level 2 revealed that the gut microbiome in responders was enriched for carbohydrate metabolism pathways and in non-responders for membrane transport pathways (Figure 7A). For carbohydrate metabolism, the pathway with the highest level of enrichment, statistical analysis showed that responders had a significantly higher level than non-responders (Figure 7B).

Discussion

To date, the literature studying the effects of dietary fibre intake or manipulation of the gut microbiota on tumour growth is limited. Wei *et al* showed that dietary fibre and the associated butyrate production reduced subcutaneous lymphoma tumour growth with associated upregulation of histone 3 acetylation (5). Hardman *et al* found slower growth of breast cancer xenografts in mice fed with fish oil concentrate (14). In contrast, Cougnoux *et al* found that Colibactin-producing *E. coli* enhanced tumour growth of colon cancer xenografts (15).

In this study, faecal and caecal microbiomes were investigated in mice fed the following: low fibre diet, low fibre diet with butyrate, high mixed fibre diet, high insoluble fibre (cellulose) diet and high soluble fibre (inulin) diet, and profiles of both microbiomes were correlated. The gut microbiomes were shaped by the different modified diets within two weeks and homogeneous gut microbiomes were seen in samples within groups. A distinct bacterial taxon was seen in each group: enrichment of *B. acidifaciens* in soluble HF, *Parabacteroides* in LF, *Akkermansia muciniphila* in LF with butyrate, and *Lachnospiraceae* in mixed HF.

The tumours were irradiated when they reached a volume of 50 mm^3 (with no effect on diet on the time to reach this point) and monitored until they reached 350 mm^3. During the course of the study, all mice developed an increased relative abundance of S24-7 family bacteria, thus indicating that their gut microbiomes had altered over the tumour growth period. Although the gut microbiomes became more heterogeneous, a notable cluster effect still existed in samples within groups. Mice responding to radiation in the soluble HF

group were enriched with *B. acidifaciens* and non-responding mice were enriched with the *Parabacteroides* genus.

A predictive metagenomics study of the gut microbiome in responders was enriched for carbohydrate metabolism pathways. This implies a higher level of fibre fermentation occurring in responders, reflecting the selection of bacteria more able to ferment carbohydrates. This could result in more SCFA production in the faeces. Both butyrate and propionate have been proposed to increase histone deacetylase inhibition, which is a known mechanism of cellular radiosensitisation (16-18).

When the mice from different diet groups were pooled, *B. acidifaciens* abundance was positively correlated with survival time, and mice with high *B. acidifaciens* had the longest median survival times using Kaplan-Meier survival analysis. Bacteroidetes, including *B. acidifaciens*, have been proposed to produce the metabolic end products acetate, succinate and possibly propionate, but not butyrate [15, 16]. High acetate levels could act as a substrate for butyrate production, given that acetate is necessary for butyrate production, particularly in the butyryl-CoA:acetate CoA-transferase pathway (19,20). We speculate that the faecal butyrate levels could have been enhanced due to cross-feeding of butyrate-producing bacteria by *B. acidifaciens*. Proof-of-concept was previously demonstrated for this by cross-feeding acetate-producing bacteria (*Faecalibacterium prausnitzii*) and butyrate-producing bacteria (*Bifidobacterium adolescentis*) (21). Of note, Ramirez-Farias *et al* showed that inulin increased both *Faecalibacterium prausnitzii* and *Bifidobacterium adolescentis* in a human volunteer study (22).

A modified gut microbiota can augment the efficacy of anti-tumoral treatment. However, most studies to date are limited to chemotherapy and immunotherapy, reviewed in (23,24). Recently, Herranz *et al* found that depletion of gram positive bacteria in the gut by vancomycin enhanced radiotherapy-induced anti-tumour immune response and further delayed tumour growth. However, the authors gave very large 21 Gy single fraction irradiation doses. Furthermore, reductions in abundance/absence of gram negative bacteria (including *Bacteroides* and *S24-7*) were also seen, with increased *Parabacteroides*, which could be of significance. Here we only gave a 6 Gy single fraction of IR which is more clinically relevant, and our findings were not immunologically-mediated via T cells, as CD1 nude mice lack T cells.

To our knowledge, ours is the first study to provide evidence that a high soluble fibre diet, and its subsequent modification of the gut microbiome, can act to radiosensitise tumours.

Furthermore, *B. acidifaciens* was identified as a potential radiosensitiser because its abundance was enhanced by a high soluble fibre diet and positively correlated with tumour response to radiation and survival time in the IR cohort. This bacterium was first isolated in 2000 and was so named because it reduces the pH level of peptone-yeast broth with Fildes' digest (13). Consistent with our findings, Marques *et al* demonstrated that a high-fibre diet markedly increased the prevalence of *B acidifaciens* (25). Another study showed *B. acidifaciens* to be enriched in normal human subjects, compared to patients with inflammatory bowel disease (26), and *B. acidifaciens* increased insulin sensitivity and prevented further obesity (27). However, the effect of this bacteria on tumour growth is still controversial. A study found increased *B. acidifaciens* abundance associated with

hepatocellular carcinoma induced by a streptozotocin-high fat diet (28). In contrast, *B. acidifaciens* reduces the isoflavone genisten, which is associated with increased risk of breast cancer (29) and *B. acidifaciens* was shown to contribute to the anti-tumour effect of medicinal Gynostemma saponins (30).

We also found *Bacteroidales S24-7* (or *Candidatus Homeothermaceae* (31) or *Muribaculaceae* (32)), an uncultured bacterium with limited characterisation, to be highly abundant in our study, especially in the mixed HF and soluble HF group. The prevalence of this bacterium in humans is 20% (33). However, increased prevalence of *Bacteroidales S24-7* of up to 70% has been shown in the Hadza tribe of Tanzania who consume tubers containing large amounts of soluble fibre (33). This indicates that high abundance of *Bacteroidales S24-7* found in this study when the tumours reached 350 mm^3 might be induced by soluble high fibre.

Environmental contamination is an inevitable issue in microbiome studies (34). To minimise the influence of contamination in this study, bacterial loads of samples were quantified and appropriate negative controls were included. Bacterial loads from luminal contents and tissue samples contained more than 10^4 CFUs which overrode the environmental bacteria communities. Furthermore, the bacterial compositions of the PBS negative controls were very different from those of the study groups, so the environmental microbiome was considered not to be a major source of bias in this study.

Although a strong correlation between *B. acidifaciens* abundance and tumour response to irradiation was seen, further studies are needed to determine the causal relationship

between *B. acidifaciens* and radiosensitisation, and its underlying aetiology. This could be achieved by oral gavage of *B. acidifaciens* with or without other bacteria in gnotobiotic mice and *in vitro* culture studies of *B. acidifaciens.* As both gut bacteria (35) and irradiation (36) directly interact with the immune system, further *in vivo* studies need to be conducted in an immune competent model to reveal how immunomodulation might contribute to the radiosensitisation.

In summary, a high soluble fibre diet increased responses of RT112 subcutaneouse xenografts in CD1 nude mice to irradiation and this phenotype was associated with higher relative abundance of *B. acidifaciens*. Possible mechanisms mediating this effect, which require further investigation, include: (1) increased concentrations of metabolites, including butyrate or other short-chain fatty acids in tumours, acting via HDAC inhibition or via other pathways; (2) suppression of overgrowth of unfavourable bacteria, such as *Parabacteroides* genus; and/or (3) enhancement of anti-tumoral immunity. Our findings suggest that dietary fibre modification and the resultant modification of the gut microbiome might be exploited to improve tumour responses to radiotherapy in human patients.

Methods

Mice and mouse diets

All animal procedures were performed in accordance with the ARRIVE guidelines. CD1-nude female mice (Charles River Laboratories, USA 6-7 weeks) were housed in a temperature-controlled environment with a 12-h reversed-phase light/dark cycle (lights on 21:00 h) and provided with food and water *ad libitum*. Mice were randomised in Excel using the RAND function into four groups. At 7 to 8 weeks of age, mice were injected subcutaneously with RT112 bladder cancer cells (DSMZ, Germany) and started receiving either a low fibre diet (2 g cellulose/3850 kcal), a high insoluble fibre diet (100 g cellulose/3850 kcal), a high soluble fibre diet (100 g inulin/3850 kcal) or a high mixed fibre diet (50 g cellulose + 50 g inulin / 3850 kcal) for a maximum time of 9 weeks or until they were culled when the tumours reached 350 mm^3. Faeces, caecal contents, and proximal and distal colons from the first cohort were taken when the tumour reached 50 mm^3 (each group n=3) without irradiation to investigate the microbiome at baseline. Faeces and caecal contents from the second cohort were taken when the tumour reached 350 mm^3 after IR (each group n=8) or without IR (each group n=3) or at the end of study (9 weeks after xenograft) to study the association between the gut microbiome composition and tumour response.

Xenograft model and irradiation method

Mice were injected subcutaneously under anaesthesia into the right flank with 5 x 10^6 human bladder cancer cells (RT112) in RPMI medium (Sigma Aldrich) with phenol red-free Matrigel (BD Biosciences) at a total volume of 100 μl (1:1 ratio cell suspension to Matrigel). Tumour growth was measured three times a week and size determined by calipers using (length x width x height x π/6). To assess the effects of different dietary fibres on tumour growth after irradiation *in vivo*, mice received ionising radiation to the tumour (6 Gy, single

fraction, 300 kV, using a Gulmay-320 cabinet irradiator, Xstrahl Inc, UK). A dose of 6 Gy was chosen due to the promising effect in our previous radiosensitisation experiments with a HDAC inhibitor (manuscript in preparation.)

Microbiome sample collection and DNA extraction

All samples were transported on ice and kept at -20°C for less than 2 hours before DNA extraction. Bacterial genomic DNA was extracted using a DNeasy PowerSoil DNA Isolation Kit (QIAGEN Ltd, Manchester, UK), as per the Human Microbiome Project (37). Briefly, by adding sodium dodecyl sulfate (SDS), microbial cells were lysed by mechanical disruption with a ceramic bead set on 3,000 rpm for 10 minutes, followed by binding of DNA tightly to a silica membrane in a Spin Filter device at high salt concentrations. Eventually, DNA was collected into sterile elution buffer and quantified using a NanoDrop spectrophotometer. All DNA samples were kept at -80°C. All samples were collected and handled in sterile containers and equipment to minimise contamination. Those sent for sequencing (Omega Bioservices,Georgia, USA) were dried in an Eppendorf concentrator 5301 (Eppendorf North America Inc, USA) at a rotational speed of 1,400 rpm and centrifugal force of 240 x g for 1 hour at 30°C.

Faecal butyrate levels quantification

Faecal samples were first homogenised in ice cold Millipore Synergy purified water. Thereafter, 20 µL of sample or standard was taken and 10 µL of internal standard (valeric acid, Alfa Aesar, UK) added prior to the addition of 5 µL 15% percholoric acid. Samples were mixed and centrifuged at 12,000 g for 15 min at 4°C followed by direct injection (10 µL) of the supernatant. High-performance liquid chromatography (HPLC) separation was carried out using a Waters Acquity H-Class Quarternary Solvent Manager with mobile phases of 0.1% formic acid in water (A) and methanol (B) and a gradient of 35-75% B on a Waters

Acquity CSH C18, 1.7 µm, 100 x 2.1 column. Butyrate and internal standard (IS) were detected by mass spectrometry with a Waters Acquity TQ detector in positive electrospray ionisation mode. Butyrate was detected with a cone voltage of 20 V at selected ion recording (SIR) of *m/z* 88.41 (M+H) and IS with a cone voltage of 15 V and SIR of *m/z* 103.2 (M+H).

Identification and quantification of bacterial DNA

The microbiota of the contents of the intestinal tracts and the intestinal wall of the proximal and distal colon (tissue) was quantified by PCR of 16S rRNA. This was performed on genomic DNA extracted as described above. The PCR was performed using primers - V3F (CCAGACTCCTACGGGAGGCAG) and V3R (CGTATTACCGCGGCTGCTG) (38). All primers were purchased from Sigma. For each sample, Phire Tissue Direct PCR Master Mix (Thermo Fisher Scientific) was used to amplify the 16S rRNA gene hypervariable V3 region (product size = 200 bp). PCR amplifications were performed using the following conditions: 98°C for 5 minutes followed by 35 cycles at 98°C for 5 seconds each, 66.3°C for 5 seconds, and 72°C for 30 seconds and a final extension step at 72°C for 1 minute. The amplification products were visualised on a 1% agarose gel after electrophoretic migration of 5 µl of amplified material. A standard curve was created from serial dilutions of *Escherichia Coli* from 1 x 10^2, 1 x 10^4, 1 x10^6 colony-forming units (CFU) which was quantified by CFU assay. All samples were run in duplicate. In CFU assay, 20 µL of serial dilution of *E. Coli* was incubated onto Luria-Bertani (LB) agar plates, and colonies were counted and bacterial concentrations of the original samples were estimated after 24 hours incubation.

Bacterial 16S rRNA gene sequencing

16S rRNA gene sequencing methods were adapted from the methods developed for the NIH-Human Microbiome Project (37,39). Raw 16S rRNA reads and metadata have been

made available in Figshare (https://figshare.com/projects/The_gut_microbiota_may_drive_the_radiosensitising_effect_of_a_high_fibre_diet/68393). The amplification and sequencing of 16S rRNA gene V3V4 region were done commercially by Omega Bioservices (Georgia, USA) on a MiSeq platform (Illumina, Inc, San Diego, CA) using the 2x300 bp paired-end protocol, yielding paired-end reads with near-complete overlap. The primers containing adapters for Miseq sequencing were used for amplification and single-end barcodes, allowing pooling and direct sequencing of PCR products (40). PBS negative controls were included to eliminate the confounding effects of environmental contamination.

All 16S rRNA gene-based metagenomic analysis was conducted using a QIIME2 platform (41). Quality filtered sequences with >97% identity were clustered into bins known as Operational Taxonomic Units (OTUs), using open-reference OTU picking. The relative abundance of each OTU was obtained from all samples. In the taxonomic analysis, the microbiome at the phylum, class, order, family, genus and species levels was classified with reference to the Greengenes database (42).

The analysis pipeline was as follows:

i. All sequences were trimmed to a length of 240, since the quality dropped above this length based on the sequence quality plots.
ii. De-noised sequencing errors by using the “Deblur” plugin in QIIME2 (43).
iii. Taxonomic assignment was performed with Greengenes (44) by the “feature-classifier” command.
iv. To visualise the differences in microbial composition between gut contents and tissue, a taxonomic profile was generated by conducting differential abundance analysis using balances in gneiss.

v. To identify the features characterising the differences between groups, the LEfSe method of analysis was performed to compare abundances of all bacterial clades (45). By validation using the Kruskal-Wallis test at the α setting of 0.05, effect size was obtained by LDA (linear discriminant analysis) based on the significantly different vectors resulting from the comparison of abundances between groups.

vi. To validate the significance of enrichment of bacterial taxa among different groups, discrete false-discovery rates (DS-FDR) were calculated (46)

vii. A phylogenetic tree was generated by using the "phylogeny" plugin in QIIME2.

viii. To investigate the alpha and beta diversity, the diversity commands of "alpha-group-significance" and "beta-group-significance" were used to obtain Shannon's index, and Bray-Curtis dissimilarity. A principal coordinates (PCoA) plot was obtained by using the Emperor Tool based on the results of Bray-Curtis dissimilarities.

ix. The OTU table was rarefied using the "alpha-rarefraction" command in QIIME2. The alpha rarefraction plot showed the richness of the samples with increasing sequence count.

x. To predict the metagenome functional profiles, PICRUSt, a bioinformatics software package, was used to collapse predicted functions (KEGG Orthology; KO) based on 16S rRNA surveys into higher categories (KEGG pathway) after picking OTUs and normalisation (47).

Statistics

Power calculations for the number of mice per group were done using G*Power software version 3.1.9.4 (48). Alpha diversity and relative abundance of specific bacterial taxa were

compared using the Kruskal-Wallis test following by Dunn's multiple comparison test. All mice were classified into high, intermediate or low diversity groups based on tertiles of distribution. Time to treble in volume was defined as the interval (in days) from the date of irradiation (growth to 50 mm^3) to the date for the tumour to treble in volume. Tumour growth curves were analysed for each group, and their slopes were compared using one-way ANOVA. The LEfSe method of analysis was applied to determine the difference in bacterial taxa, using the Kruskal-Wallis test. Significantly different taxa presented from the previous comparison applying LEfSe method were used as input for LDA, which produced an LDA score. Volcano plots showed the significance of the taxa which are different among different groups, with $\log_{10}$ (FDR-adjusted p-values) on the y-axis and median-adjusted effect sizes on the x-axis. In addition, mice were also classified as having high, intermediate and low abundance of *B. acidifaciens* or high and low abundance of *parabacteroides* genus based on the relative abundance of these taxa in the gut microbiome sample. All analyses were conducted in QIIME2 and GraphPad Prism version 8.0 (La Jolla, CA).

Study approval

All animal protocols were approved by the University of Oxford Clinical Medicine Animal Welfare Ethics Review Board and conducted under animal project licences (PPL) P4B738A3B and P8484EDAE.

Declarations

Authors' contributions

CKT extracted the DNA from mouse samples, performed the analysis and interpretation of the data and drafted the manuscript. SP performed the animal experiments, collected the faeces, caecal contents, intestinal tissue and blood. AH measured the faecal butyrate levels. AEK conceived the study, supervised the work, and revised the manuscript. All authors read and approved the final manuscript.

Acknowledgements

This work was funded by Cancer Research UK Programme grant C5255/A15935. The funding body had no role in the design of the study, collection, analysis, interpretation of data or in writing the manuscript. We thank Professor Simon Kroll and Dr Anderson Ryan for their very helpful comments. We thank Dr Jia-Yu Ke at Research Diets, Inc. for formulation of the mouse diets, Dr Lisa Folkes for assistance with the faecal butyrate quantification and Omega Bioservices (Georgia, USA) for the 16S rRNA gene sequencing on a MiSeq platform.

References

1. Viswanathan AN, et al. Complications of pelvic radiation in patients treated for gynecologic malignancies. *Cancer.* 2014;120(24):3870-3883.
2. Nishimura Y. Rationale for chemoradiotherapy. *Int J Clin Oncol.* 2004;9(6):414-420.
3. Wedlake L, et al. Randomized controlled trial of dietary fiber for the prevention of radiation-induced gastrointestinal toxicity during pelvic radiotherapy. *Am J Clin Nutr.* 2017;106(3):849-857.
4. Hedelin M, et al. Intake of citrus fruits and vegetables and the intensity of defecation urgency syndrome among gynecological cancer survivors. *PLoS One.* 2019;14(1):e0208115.
5. Wei W, Sun W, Yu S, Yang Y, Ai L. Butyrate production from high-fiber diet protects against lymphoma tumor. *Leuk Lymphoma.* 2016;57(10):2401-2408.
6. David LA, et al. Diet rapidly and reproducibly alters the human gut microbiome. *Nature.* 2014;505(7484):559-563.
7. Trompette A, et al. Dietary Fiber Confers Protection against Flu by Shaping Ly6c(-) Patrolling Monocyte Hematopoiesis and CD8(+) T Cell Metabolism. *Immunity.* 2018;48(5):992-1005 e1008.
8. Bachem A, et al. Microbiota-Derived Short-Chain Fatty Acids Promote the Memory Potential of Antigen-Activated CD8(+) T Cells. *Immunity.* 2019;51(2):285-297 e285.
9. Kim M, Friesen L, Park J, Kim HM, Kim CH. Microbial metabolites, short-chain fatty acids, restrain tissue bacterial load, chronic inflammation, and associated cancer in the colon of mice. *Eur J Immunol.* 2018;48(7):1235-1247.
10. Deehan EC, et al. Precision Microbiome Modulation with Discrete Dietary Fiber Structures Directs Short-Chain Fatty Acid Production. *Cell Host Microbe.* 2020.
11. Basson AR, Wijeyesekera A. Metabolic phenotyping for understanding the gut microbiome and host metabolic interplay. *Emerging Topics in Life Sciences.* 2017;1(4):325–332.
12. Macy JM, Probst I. The biology of gastrointestinal bacteroides. *Annu Rev Microbiol.* 1979;33:561-594.
13. Miyamoto Y, Itoh K. Bacteroides acidifaciens sp. nov., isolated from the caecum of mice. *Int J Syst Evol Microbiol.* 2000;50 Pt 1:145-148.
14. Hardman WE, Munoz J, Jr., Cameron IL. Role of lipid peroxidation and antioxidant enzymes in omega 3 fatty acids induced suppression of breast cancer xenograft growth in mice. *Cancer Cell Int.* 2002;2(1):10.
15. Cougnoux A, et al. Bacterial genotoxin colibactin promotes colon tumour growth by inducing a senescence-associated secretory phenotype. *Gut.* 2014;63(12):1932-1942.
16. Donohoe DR, Collins LB, Wali A, Bigler R, Sun W, Bultman SJ. The Warburg effect dictates the mechanism of butyrate-mediated histone acetylation and cell proliferation. *Mol Cell.* 2012;48(4):612-626.
17. Groselj B, Sharma NL, Hamdy FC, Kerr M, Kiltie AE. Histone deacetylase inhibitors as radiosensitisers: effects on DNA damage signalling and repair. *Br J Cancer.* 2013;108(4):748-754.
18. Silva LG, Ferguson BS, Avila AS, Faciola AP. Sodium propionate and sodium butyrate effects on histone deacetylase (HDAC) activity, histone acetylation, and inflammatory gene expression in bovine mammary epithelial cells. *J Anim Sci.* 2018;96(12):5244-5252.

19. Vital M, Howe AC, Tiedje JM. Revealing the bacterial butyrate synthesis pathways by analyzing (meta)genomic data. *MBio.* 2014;5(2):e00889.
20. Vital M, Karch A, Pieper DH. Colonic Butyrate-Producing Communities in Humans: an Overview Using Omics Data. *mSystems.* 2017;2(6).
21. Rios-Covian D, Gueimonde M, Duncan SH, Flint HJ, de los Reyes-Gavilan CG. Enhanced butyrate formation by cross-feeding between Faecalibacterium prausnitzii and Bifidobacterium adolescentis. *Fems Microbiol Lett.* 2015;362(21).
22. Ramirez-Farias C, Slezak K, Fuller Z, Duncan A, Holtrop G, Louis P. Effect of inulin on the human gut microbiota: stimulation of Bifidobacterium adolescentis and Faecalibacterium prausnitzii. *Brit J Nutr.* 2009;101(4):541-550.
23. Alexander JL, Wilson ID, Teare J, Marchesi JR, Nicholson JK, Kinross JM. Gut microbiota modulation of chemotherapy efficacy and toxicity. *Nat Rev Gastroenterol Hepatol.* 2017;14(6):356-365.
24. Gopalakrishnan V, et al. Gut microbiome modulates response to anti-PD-1 immunotherapy in melanoma patients. *Science.* 2018;359(6371):97-103.
25. Marques FZ, et al. High-Fiber Diet and Acetate Supplementation Change the Gut Microbiota and Prevent the Development of Hypertension and Heart Failure in Hypertensive Mice. *Circulation.* 2017;135(10):964-977.
26. Ott SJ, et al. Reduction in diversity of the colonic mucosa associated bacterial microflora in patients with active inflammatory bowel disease. *Gut.* 2004;53(5):685-693.
27. Yang JY, et al. Gut commensal Bacteroides acidifaciens prevents obesity and improves insulin sensitivity in mice. *Mucosal Immunol.* 2017;10(1):104-116.
28. Xie G, et al. Distinctly altered gut microbiota in the progression of liver disease. *Oncotarget.* 2016;7(15):19355-19366.
29. Renouf M, Hendrich S. Bacteroides uniformis is a putative bacterial species associated with the degradation of the isoflavone genistein in human feces. *J Nutr.* 2011;141(6):1120-1126.
30. Chen L, Tai WC, Brar MS, Leung FC, Hsiao WL. Tumor grafting induces changes of gut microbiota in athymic nude mice in the presence and absence of medicinal Gynostemma saponins. *PLoS One.* 2015;10(5):e0126807.
31. Ormerod KL, et al. Genomic characterization of the uncultured Bacteroidales family S24-7 inhabiting the guts of homeothermic animals. *Microbiome.* 2016;4.
32. Lagkouvardos I, et al. Sequence and cultivation study of Muribaculaceae reveals novel species, host preference, and functional potential of this yet undescribed family. *Microbiome.* 2019;7(1):28.
33. Ormerod KL, et al. Genomic characterization of the uncultured Bacteroidales family S24-7 inhabiting the guts of homeothermic animals. *Microbiome.* 2016;4(1):36.
34. Eisenhofer R, Minich JJ, Marotz C, Cooper A, Knight R, Weyrich LS. Contamination in Low Microbial Biomass Microbiome Studies: Issues and Recommendations. *Trends Microbiol.* 2019;27(2):105-117.
35. Lazar V, et al. Aspects of Gut Microbiota and Immune System Interactions in Infectious Diseases, Immunopathology, and Cancer. *Front Immunol.* 2018;9:1830.
36. Carvalho HA, Villar RC. Radiotherapy and immune response: the systemic effects of a local treatment. *Clinics (Sao Paulo).* 2018;73(suppl 1):e557s.
37. Human Microbiome Project C. A framework for human microbiome research. *Nature.* 2012;486(7402):215-221.

38. Wang HY, et al. Comparative analysis of microbiome between accurately identified 16S rDNA and quantified bacteria in simulated samples. *J Med Microbiol.* 2014;63:433-440.
39. Human Microbiome Project C. Structure, function and diversity of the healthy human microbiome. *Nature.* 2012;486(7402):207-214.
40. Caporaso JG, et al. Ultra-high-throughput microbial community analysis on the Illumina HiSeq and MiSeq platforms. *ISME J.* 2012;6(8):1621-1624.
41. Hall M, Beiko RG. 16S rRNA Gene Analysis with QIIME2. *Methods Mol Biol.* 2018;1849:113-129.
42. Balvociute M, Huson DH. SILVA, RDP, Greengenes, NCBI and OTT - how do these taxonomies compare? *Bmc Genomics.* 2017;18.
43. Nearing JT, Douglas GM, Comeau AM, Langille MGI. Denoising the Denoisers: an independent evaluation of microbiome sequence error-correction approaches. *Peerj.* 2018;6.
44. DeSantis TZ, et al. Greengenes, a chimera-checked 16S rRNA gene database and workbench compatible with ARB. *Appl Environ Microb.* 2006;72(7):5069-5072.
45. Segata N, et al. Metagenomic biomarker discovery and explanation. *Genome Biology.* 2011;12(6).
46. Jiang L, Amir A, Morton JT, Heller R, Arias-Castro E, Knight R. Discrete False-Discovery Rate Improves Identification of Differentially Abundant Microbes. *mSystems.* 2017;2(6).
47. Langille MG, et al. Predictive functional profiling of microbial communities using 16S rRNA marker gene sequences. *Nat Biotechnol.* 2013;31(9):814-821.
48. Faul F, Erdfelder E, Lang AG, Buchner A. G*Power 3: A flexible statistical power analysis program for the social, behavioral, and biomedical sciences. *Behav Res Methods.* 2007;39(2):175-191.

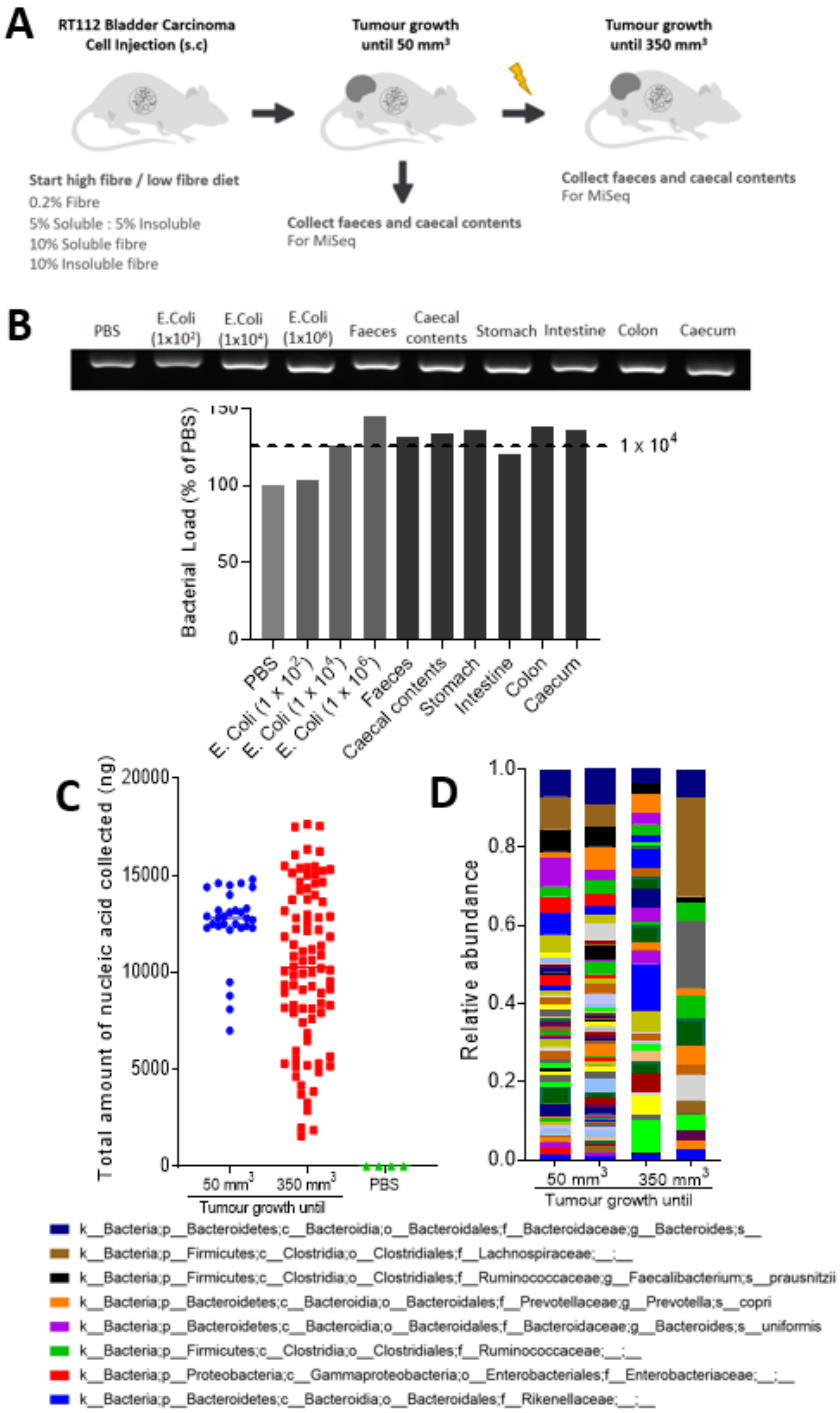

Figure 1. The environmental microbiome had minimal impact on gut microbiome analysis. (A) Two microbiomes were analysed from the intestinal tract, namely, faecal and caecal content samples collected when tumours reached 50 mm^3 and 350 mm^3 respectively. (B) Quantification of bacterial load from different tissue and luminal contents from mice, with *E. Coli* (1 x 10^2, 1 x 10^4, 1 x10^6 CFUs) as controls (n=1 mouse). (C) Comparison of the total amount of nucleic acid quantified by PicoGreen assay in all samples collected when the tumours reached 50 mm^3 and 350 mm^3. (D) Common bacterial taxa at the species level in 4 samples of PBS, as negative controls of DNA extraction by 16S rRNA sequencing.

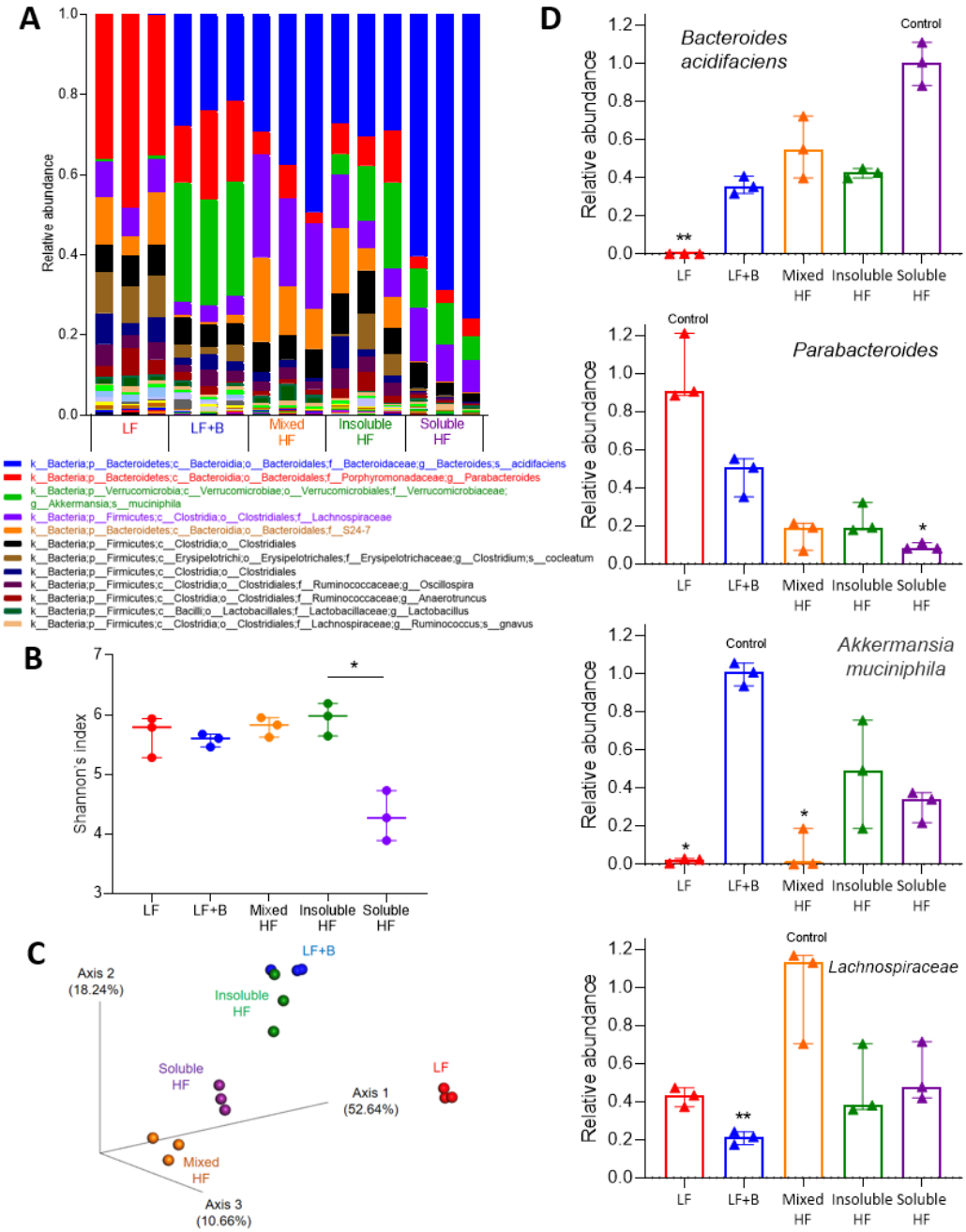

Figure 2. Dietary fibre shapes the baseline gut microbiome when tumours reached 50 mm³. (A) Stacked bar plot of phylogenetic composition of common bacterial taxa at the species level when tumours reached 50 mm³. Faeces were collected from mice fed with low fibre, low fibre with butyrate, high mixed fibre, high insoluble fibre and high soluble fibre diets (n=3 for each group). (B) Shannon's index of gut microbiomes by Kruskal-Wallis test. Error bars represent the interquartile range of diversity scores. (C) Principal coordinate analysis of gut microbiomes using Bray-Curtis dissimilarity. A notable clustering effect by diet was seen in the gut microbiome. (D) Differentially abundant taxa when the tumours reached 50 mm³. All comparisons among different diet groups was performed by Kruskal-Wallis test and Dunn's multiple comparison tests. All tests compared each median with the 'control' denoted. The diet with the highest abundance of a taxa was denoted as the control. *P<0.05; **P<0.01.

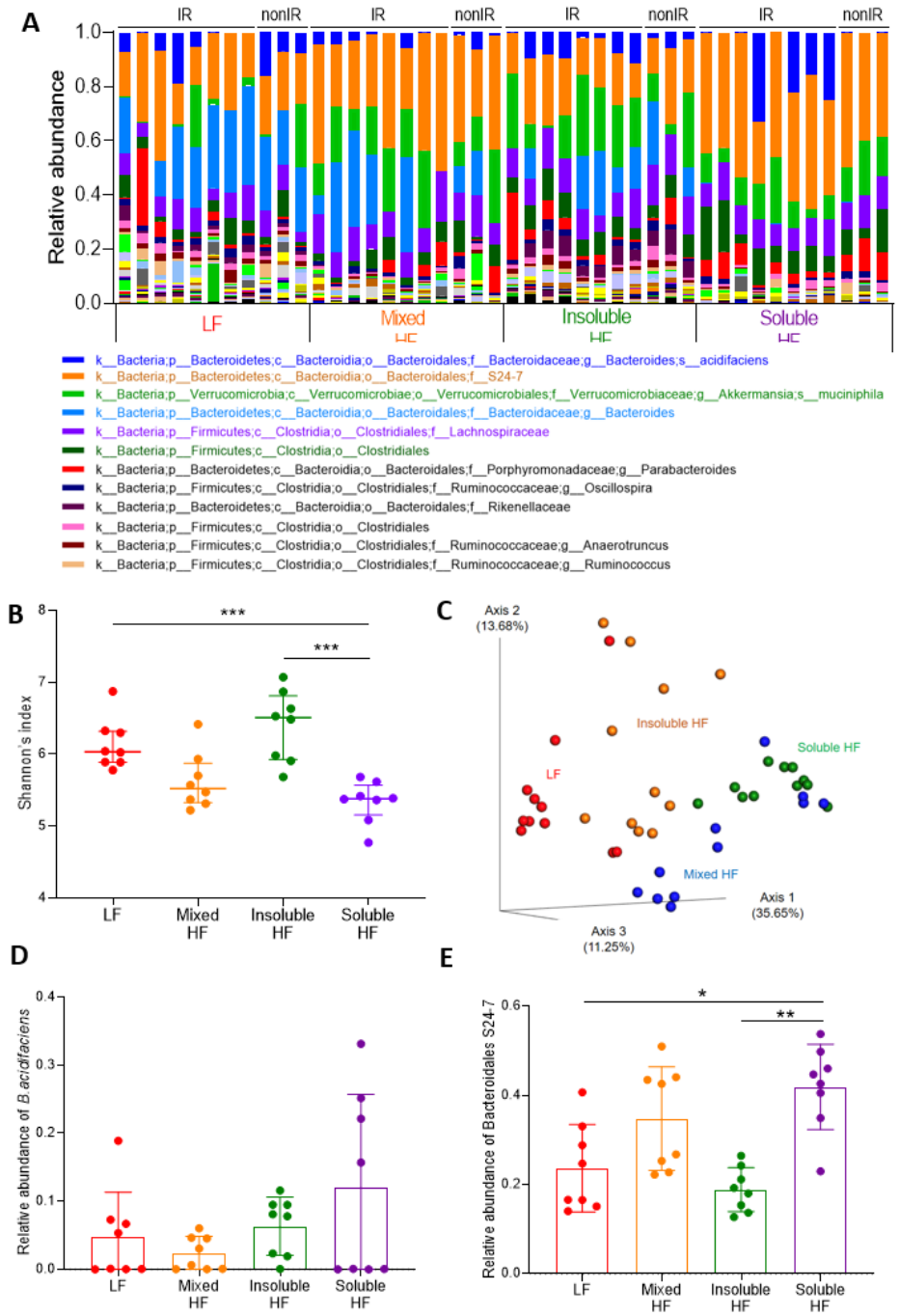

Figure 3. Composition of the gut microbiome when tumours reached 350 mm³. (A) Stacked bar plot of the phylogenetic composition of common bacterial taxa at the species level when tumours reached 350 mm³. Samples were collected from mice fed with low fibre, high mixed fibre, high insoluble fibre and high soluble fibre diets (n=8 for each group). (B to E) show results for irradiated mice only. (B) Shannon's index of gut microbiomes by Kruskal-Wallis test. Error bars represent the interquartile range of diversity scores. (C) Principal coordinate analysis of gut microbiomes using Bray-Curtis dissimilarity. Relative abundance of (D) *B. acidifaciens* and (E) *Bacteroidales S24-7* in mice with or without irradiation.

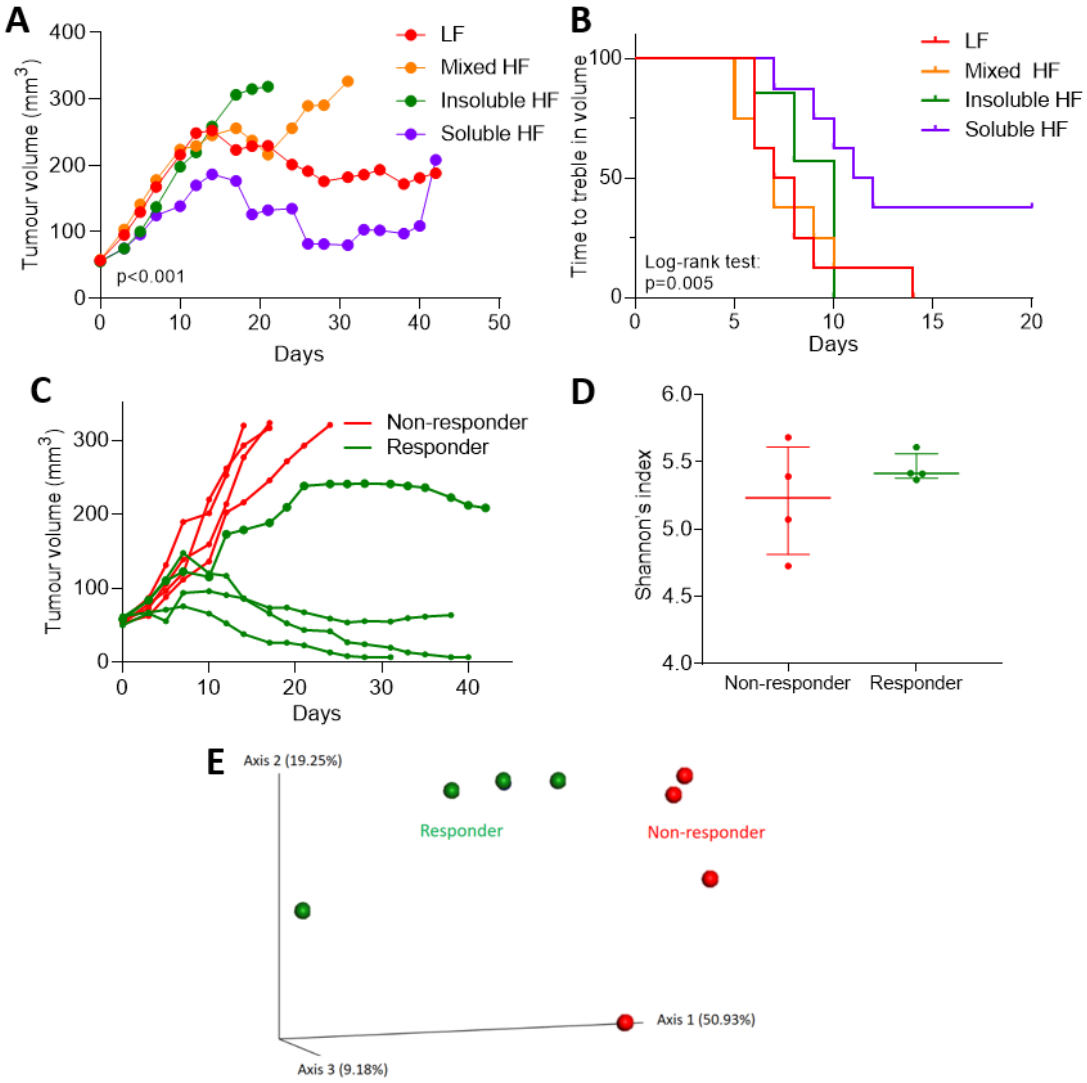

Figure 4. Soluble high fibre causes increased growth delay in irradiated bladder cancer cell xenografts and responses are influenced by gut microbiota composition. (A) Tumour growth in RT112 flank xenografts irradiated with 6 Gy IR, in mice fed low fibre, high mixed fibre, high insoluble fibre and high soluble fibre diets (n=8 for each group). Tumour curve slopes were calculated by linear regression to represent tumour growth rates and compared by ANOVA. (B) Kaplan–Meier survival curves for mice showing plots of time to treble tumour volume. (C) Mice in the soluble HF group were stratified into responders and non-responders based on tumour radiation response. (D) Shannon's index of gut microbiota in responders and non-responders by Kruskal-Wallis test. Error bars represent the interquartile range of diversity scores. (E) Principal coordinate analysis of gut samples (n=8) in the soluble HF group by response using Bray-Curtis dissimilarity.

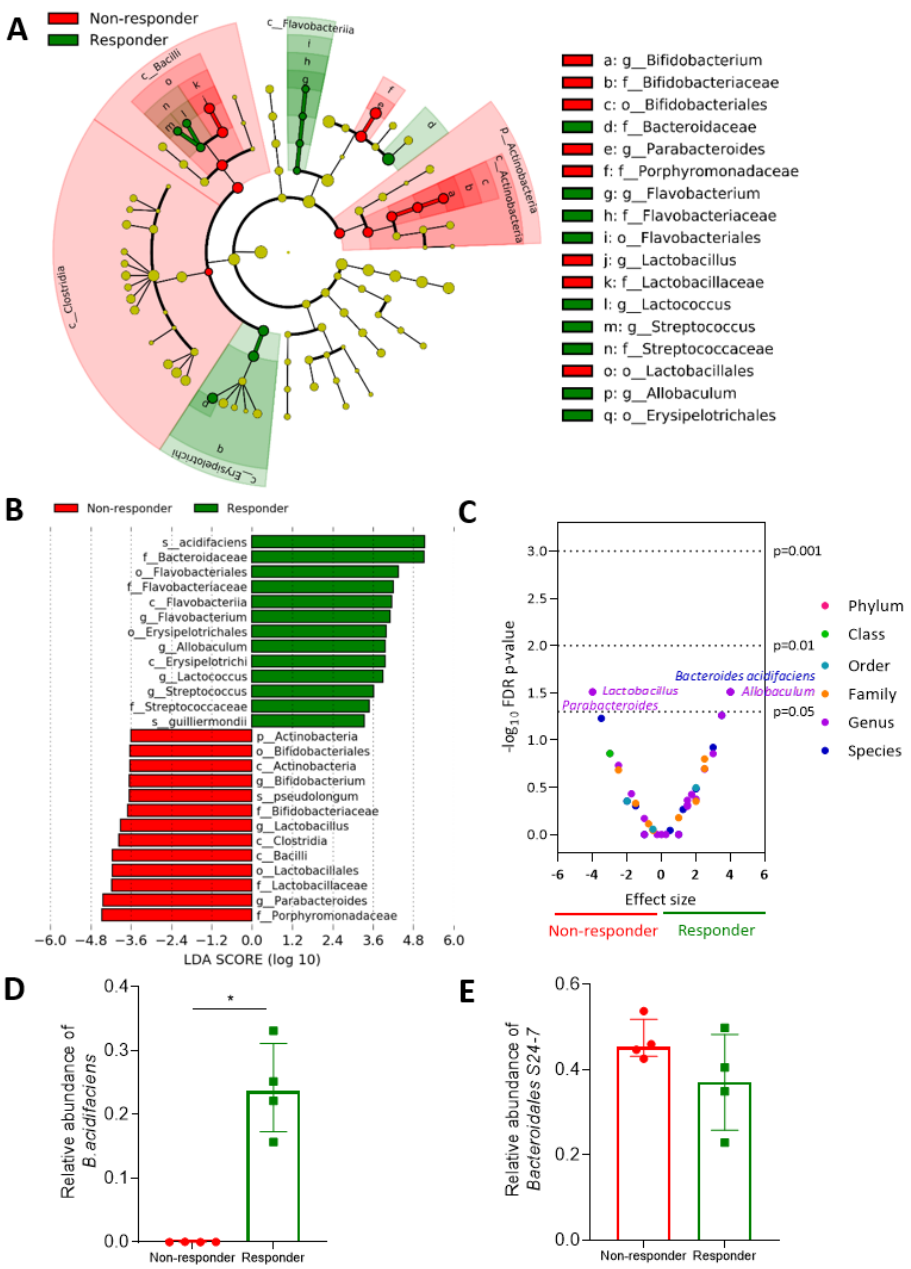

Figure 5. Differences in composition of the gut microbiome between responders and non-responders. (A) Taxonomic cladogram from LEfSe showing differences among taxa between responders and non-responders in the soluble HF group. Dot size is proportional to the abundance of the taxon. (B) Linear discriminant analysis (LDA) scores computed for differentially abundant taxa in the microbiomes of responders (green) and non-responders (red). Length indicates the effect size associated with a taxon, p=0.05 for Kruskal-Wallis test. (C) Discrete false-discovery rate of different abundant taxa in responders and non-responders in the soluble HF group. Differential abundance within all taxonomic levels in responders versus non-responders by Mann-Whitney U test. Dots are overlapping between *Bacteroides acidifaciens* and *Allobaculum*, and between *Lactobacillus* and *Parabacteroides*. Relative abundance of (D) *B. acidifaciens* and (E) *Bacteroidales S24-7* and in responders and non-responders in the soluble HF group.

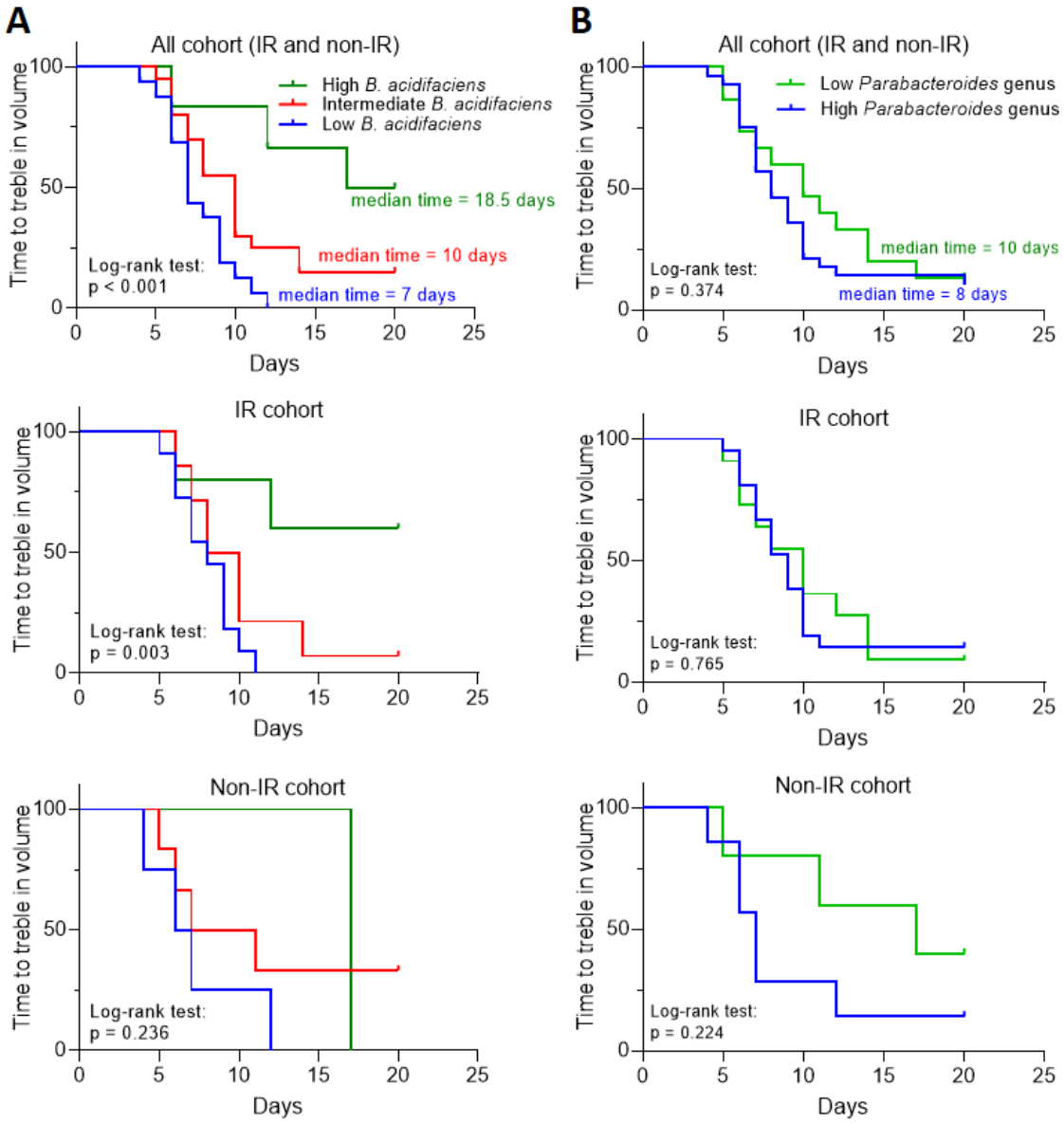

Figure 6. Abundance of OTUs within the gut microbiome is predictive of response to ionising irradiation. Kaplan-Meier (KM) plots of time for tumours to treble in volume, whole cohorts, IR cohorts, non-IR cohorts, based on (A) *B. acidifaciens* or (B) *Parabacteroides* genus abundance in IR and Non-IR cohorts from different diet groups combined. Comparison KM plots by log-rank test in mice with high abundance (green; relative abundance > 0.1), intermediate abundance (red; 0.1 > relative abundance > 0.01), or low abundance (blue; 0.01 > relative abundance) of *B. acidifaciens* in all, IR and non-IR cohorts. For *Parabacteroides* genus, relative abundance more than or equal to 0.01 was classified as high (blue), while less than 0.01 was classified as low (green).

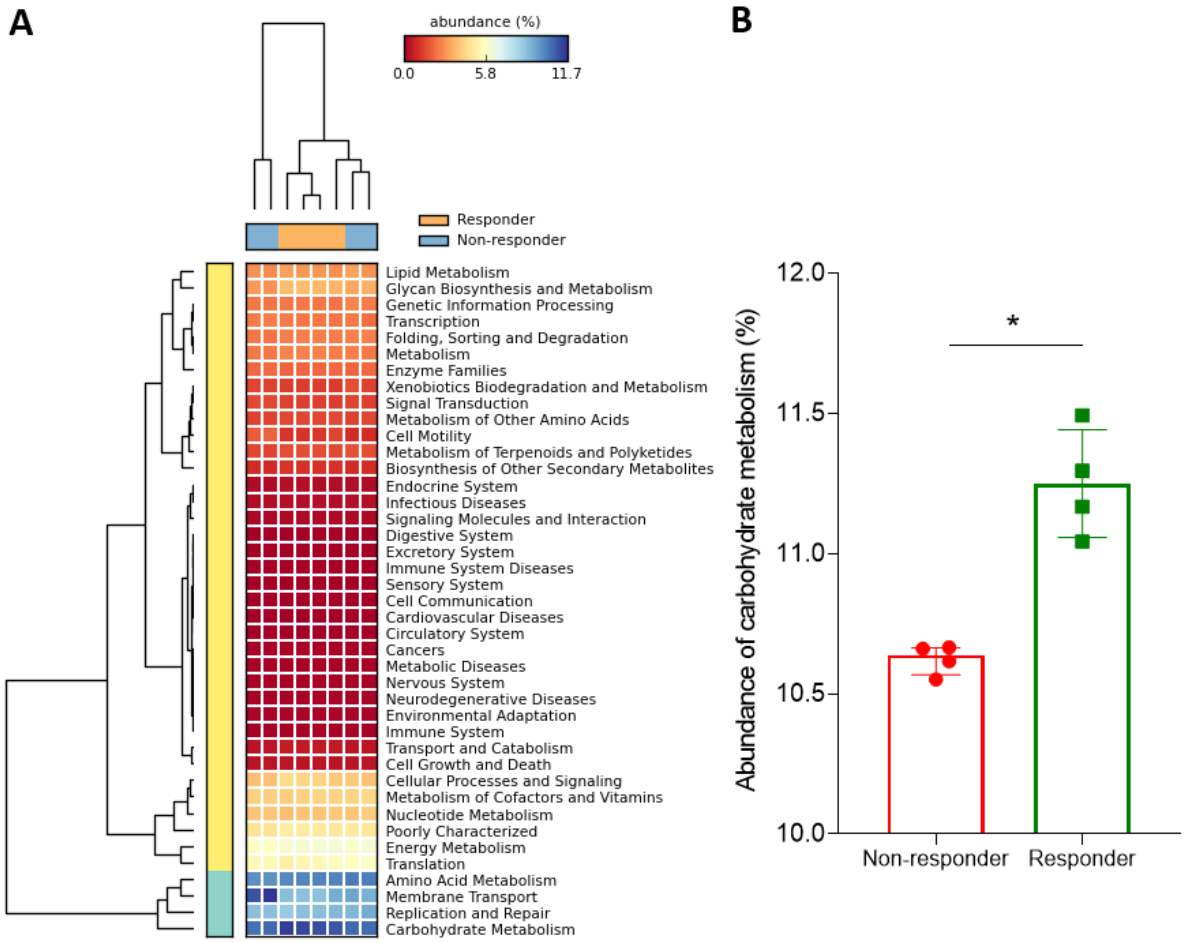

Figure 7. A favourable gut microbiome is associated with enhanced carbohydrate metabolism. Metagenomic functional prediction by PICRUSt of the gut microbiome in responders (n=4) and non-responders (n=4) in the soluble HF group with reference to the KEGG database level 2. Columns represent mice (responders, orange; non-responders, blue), and rows represent enrichment of predicted KEGG pathways (red, low enrichment; yellow, medium enrichment; blue, high enrichment).